Journal of King Saud University – Science 33 (2021) 101409

Contents lists available at ScienceDirect

Journal of King Saud University – Science

journal homepage: www.sciencedirect.com

Original article

Biochar/polypropylene composites: A study on the effect of pyrolysis temperature on crystallization kinetics, crystalline structure, and thermal stability

Abdulaziz A. Alghyamah [a], Ahmed Yagoub Elnour [a,b], Hamid Shaikh [b,*], Sajjad Haider [a], Anesh Manjaly Poulose [b], S.M. Al-Zahrani [a,b], Waheed A. Almasry [a], Soo Young Park [c]

[a] Chemical Engineering Department, College of Engineering, King Saud University, Riyadh 11421, Saudi Arabia
[b] SABIC Polymer Research Centre (SPRC), Chemical Engineering Department, King Saud University, P. O. Box 800, Riyadh 11421, Saudi Arabia
[c] Department of Polymer Science & Engineering, Polymeric Nanomaterials Laboratory, School of Applied Chemical Engineering, Kyungpook National University, 80 Daehak-ro, Buk-gu, 41566 Daegu, Republic of Korea

ARTICLE INFO

Article history:
Received 18 February 2021
Revised 9 March 2021
Accepted 9 March 2021
Available online 22 March 2021

Keywords:
Biochar
Polypropylene
Polymer composites
Crystallization behavior
Thermal stability
Avrami model

ABSTRACT

The crystallization behavior of polyolefins continues to gain much attention for the prediction of suitable processing conditions. This study aims to understand the influence of biochar (BC) particles on the crystallization behavior of the selected semi-crystalline polypropylene (PP). For this purpose, BC samples were prepared from waste biomass at various pyrolysis temperature. The prepared BC samples were used to fabricate PP composites *via* melt processing technique. The crystallization behavior of these composites was studied by differential scanning calorimetry (DSC) calorimetry and validated using Avrami analysis in a non-isothermal conditions. It was observed that BC particles act as nucleating agents and accelerate the overall rate of crystallization. Avrami theory analysis indicated that the addition of BC particles provides polypropylene (PP) composites with a higher crystallization rate, i.e. about one order of magnitude higher than the neat PP. The results of the TGA analysis showed that the BC particles enhanced the thermal stability of the BC/PP composites, and is up to 80 °C higher than the neat PP sample.

1. Introduction

Research on the use of biochar (BC) as a functional filler for the synthesis of polymer composites with improved matrix performance (or to achieve composites with new properties) is more intensified recently (Pudełko et al., 2021; Adeniyi et al., 2020; Zhang et al., 2020; Elnour et al., 2019; Giorcelli et al., 2019; Poulose et al., 2018; Behazin et al., 2017; Das et al., 2016). BC is pyrogenic carbonaceous material obtained from the biomass pyrolysis. It is carbon-rich, has a porous structure, and is considered a low-cost alternative to other expensive carbon materials such as activated carbon, carbon black, and carbon nanotubes. One of the advantages of BC as a reinforcement filler is the porous structure which induces better adhesion with the polymeric matrix. The improved interfacial adhesion is an important factor for an effective enhancement of the composite properties (Das et al., 2016; Ikram et al., 2016).

Polypropylene (PP), a semi-crystalline polyolefin thermoplastic polymer, its crystallization studies have been explored for decades, and remarkable success has been achieved, still, some answers need to be found when new and novel functional fillers are being used. The isostatic PP is commonly used for the formulation of composites due to its low density, ease of processibility, and low-cost availability. Since PP occupies almost 20% of the market and continues to grow, an investigation of the effect of particular filler on the crystallization and thermal behavior of PP in the composites could be of great importance to further utilization its application in the industry (Mileva et al., 2018). The major factors, which influence the crystalline behavior of PP are; temperature, processing parameters, and most importantly filler type (inorganic

* Corresponding author.
E-mail addresses: aalghyamah@ksu.edu.sa (A.A. Alghyamah), aelnour@ksu.edu.sa (A. Yagoub Elnour), shaider@ksu.edu.sa (H. Shaikh), hamshaikh@ksu.edu.sa (S. Haider), apoulose@ksu.edu.sa (A. Manjaly Poulose), szahrani@ksu.edu.sa (S.M. Al-Zahrani), walmasry@ksu.edu.sa (W.A. Almasry), psy@knu.ac.kr (S. Young Park).

Peer review under responsibility of King Saud University.

Production and hosting by Elsevier

https://doi.org/10.1016/j.jksus.2021.101409
1018-3647/

and organic carbonaceous material). Furthermore, the intrinsic properties of the filler such as surface functionality, aspect ratio, loading amount, and nucleating ability also have a significant impact on the crystallization of PP in the composites (Turgut et al., 2018; Wang et al., 2018; Yu et al., 2018; Zheng and Chen, 2017; Cai and Dou, 2019).

In one of the recent studies, the crystallization behavior of PP reinforced with carbon nanotubes (CNTs) of varying length was investigated. CNTs have been shown to act as a nucleating agent and speed up the crystallization process. The shorter CNTs accelerated crystallization more than the longer ones as per Avrami analysis. However, thermal stability was found to improve by the longer CNTs (Lin et al., 2018). Similarly, the crystallization behavior of PP reinforced with graphene nanoplatelets was also studied. It was shown that these particles exhibit a nucleating effect due to the available particle surface for heterogeneous nucleation. This resulted in the orientation of the epitaxial growth of the alpha crystalline phase of the PP (Beuguel et al., 2018).

Although other carbons such as nanotubes (CNTs) and fibers have specific shapes and sizes, hence; the microstructure of the resultant composites and their and properties can be predicted. BC (prepared *via* pyrolysis) particles are irregular in shape, rigid in texture, and porous. Thus, their effect on the microstructure of the polypropylene (PP) and the resulting crystallization behavior needs to be studied. This is evaluated through the study of the structure–property relationship of the BC/PP composite. Therefore, in this work, BC particles with random shape were prepared at different pyrolysis temperatures. The particles were then incorporated in various loading into the PP matrix by melt blending to analyze morphology, crystalline behavior, and thermal stability of these composites.

2. Experimental

2.1. Materials

The polymer matrix used in this study for the preparation of the composite was an isotactic homopolymer polypropylene (LADENE PP570P) pellets obtained from the Saudi Basic Industries Corporation (SABIC, Saudi Arabia). This resin has a melt flow index (MFI) of 8 g/10 min (at 230 °C and 2.16 kg load) and a density of 0.905 g/cm^3. The BC particles, used in this study, were prepared through the pyrolysis of date palm tree wastes. The pyrolysis process was carried out at different temperatures, and under inert atmosphere (N_2 gas flow rate of 100 ml/min), with heating rate of 10 °C/min and residence time of 4 h. The range of pyrolysis was kept in the range of 300 to 700 °C. The difference between the pyrolysis temperature was kept at 100 °C. To carry out the process an electrical muffle furnace equipped with a stainless-steel reactor, having length of 720 mm and 50 mm diameter, was used. All BC samples were milled in a home blender to reduce the particle size and sieved to <38 μm. The detailed analysis of these BC samples are given in our previous work (Elnour et al., 2019), while a summary of their particle size distributions and physicochemical characteristics are provided as supplementary information (Tables S1 and S2).

2.2. Composites preparation

The BC/PP composite samples were prepared through the melt compounding process. Before compounding, both BC and PP were dried in an oven at 110 °C for 24 h to eliminate the moisture content. Afterward, BC and PP were weighed and premixed as per the required BC loading percentages. The mixture was then introduced to a melt compounder (DSM Xplore micro-compounder, 15 cm^3, Netherlands). The composites melt compounding process was performed in a speed-controlled mode at a temperature of 190 °C, screw speed of 100 rpm, and compounding time of 3 min. At the end of the compounding, the BC/PP composites were collected, stored, used for morphological, and thermal analysis to evaluate the microstructure-properties relationship and the crystallization behavior of the composite. The compositions of the samples and their treatment temperatures different formulations are presented in supplementary information (Table S3).

2.3. Composites characterization

The tensile-fractured surface of the BC/PP composites was investigated by using scanning electron microscopy (SEM), (JEOL Model: JSM-6360A, Japan). ASTM standard samples were subjected to a tensile load with an extension rate of 50 mm/min in order to obtain a fractured specimen. The small part of the specimen was placed on the SEM stub in such a manner that the broken surface is exposed on the top side for examination. Differential scanning calorimetric (DSC) measurements were performed, for the neat PP and the BC/PP composite samples, on a Shimadzu thermal analyzer (Model: TA-60WS), according to ASTM standard method (ASTM, 2015). The DSC instrument was calibrated with pure indium (In) metal before analysis. Each sample ~ 6–7 mg was weighed carefully and placed in an aluminum pan, which was then covered with an aluminum lid and crimped prior to analysis. To eliminate the thermal history of the samples, the neat and BC/PP samples were first heated from (30 to 250 °C) at a heating rate of 10 °C/min and subsequently cooled to 30 °C at the same rate. The second heating–cooling cycle was performed right after the first cycle and on typical rate and conditions. To avoid any thermal degradation of the samples, the thermal analysis was performed under a nitrogen (N_2) atmosphere at a flow rate of 50 cm^3/min. The melting temperature, crystallization temperature, and enthalpy of melting were analyzed using the TA-60WS software package based on the second heating–cooling cycle.

To determine the degree of crystallinity of the neat PP and BC/PP composites, the measured melting enthalpy (ΔH_m) of each sample was compared to the value for 100% crystalline PP (ΔH_m^o). Then, the crystallinity percentage of each sample was calculated by using the total enthalpy method based on the following equation.

$$X_c(\%) = \frac{\Delta H_m}{(1-\phi)\Delta H_m^o} \times 100 \quad (1)$$

Where: (X_c) is the degree of crystallinity, (ΔH_m) is the sample melting enthalpy, (ΔH_m^o) is the enthalpy of melting of 100% crystalline neat PP (ΔH_m^o for PP = 207 J/g) (Wunderlich, 1990) and (ϕ) is the weight fraction of BC in the composite.

The crystallization kinetics of The neat PP and its composites were analyzed by using the well-known Avrami model given by the following equation:

$$\theta(t) = 1 - \exp\left(-k(t)t^n\right) \quad (2)$$

Where $\theta(t)$is the relative crystallinity at time t, n is the Avrami index (crystal geometry information), T is the crystallization temperature, and k is the isothermal crystallization rate constant which indicates the nucleation and growth rates.

The relative crystallinity $\theta(t)$can be defined as the area ratio for an exothermic peak at a specific time (t) divided by the total area of the exothermic peak. The relative crystallinity$\theta(t)$ at time t is given by the following equation:

$$\theta(t) = \frac{\int_{T_0}^{T}\left(\frac{dH_c}{dt}\right)dt}{\int_{T_0}^{T_\infty}\left(\frac{dH_c}{dt}\right)dt} \quad (3)$$

Where: $T_0$and $T_\infty$are the onset and end crystallization temperatures, respectively, and $\frac{dH_c}{dt}$ is the heat flow rate.

Eq. (2) above can be transformed into a linear logarithmic in the following form.

$$\ln\left[-\ln\left(1-\theta(t)\right)\right] = n\ln(t) + \ln(k) \tag{4}$$

For the crystallization kinetics, based on the experimental heating rate, the time t is related to the temperature T as follows:

$$t = \frac{T_0 - T}{\phi} \tag{5}$$

Where: T is the temperature at time t, $T_0$is the temperature at which the crystallization begins (t = 0), and ϕ is the cooling rate.

If the crystallization kinetics is following Avrami's theory well, a plot of ln $[-\ln(1-\theta(t))]$ versus ln (t) should yield a straight line with a slope n and an intercept ln (k), from which k values could be obtained.

Also from equation (2), the half-time of crystallization ($t_{1/2}$) for crystallization kinetics, which is defined as the time at which the relative crystallinity of (50%) has been achieved (Li et al., 2006), can be expressed by the following equation:

$$t_{1/2} = \left(\frac{\ln(2)}{k}\right)^{1/n} \tag{6}$$

To observe the effect of BC incorporation on the spherulite morphology of BC/PP composites, polarized light microscopy (PLM, BX51, Olympus, Japan) was used. A few fractions of samples are placed on a glass slide and heated to melt and allowed to form a film at 230 °C. The film was cooled at a rate of 40 °C/min to attain the temperature of 120 °C, where it was retained for the observation of its spherulitic evolution over time. Thermogravimetric analysis (TGA) was used to investigate the thermal stability of BC/PP composites. For determining the thermal decomposition temperature and the residual weight of the BC/PP composites. The TGA analysis was performed, according to the ASTM E1131 standard test method (ASTM, 2020), in a Shimadzu apparatus with a simultaneous DTA-TGA thermal analyzer (Model: DTG-60H). The aluminum pan was filled with ~ 10 mg of the composite sample. Subsequently, the sample was heated from the ambient temperature up to 600 °C with a heating rate of 10 °C/min. Aluminum oxide was used as reference material. The analysis was done under air atmosphere with a flow rate of (50 cm^3/min) and accordingly, the corresponding weight loss was recorded.

3. Results and discussion

3.1. Morphology study

Fig. 1 illustrates the fracture morphology of the BC/PP composites. It is well known that the filler dispersion and the filler-polymer interfacial interaction are two significant determining factors that influence the properties of the resulted composites. The fractured surface micrographs of the composites at the maximum BC loading (i.e. 20 wt%) identify the different morphological characteristics of composites. The figure showed uniform distribution of BC into the PP matrix (some BC particles are highlighted with circles in Fig. 1). Furthermore; it can be observed from Fig. 1 that the interfacial bonding is highly dependent on the BC type, as evident from the degree of pull-out of BC particles (indicated with arrows in Fig. 1). The composites made with BC prepared at higher temperatures showed less pull-out effect than those made with BC prepared at lower temperatures. This indicates that the interface adhesion between BC particles and the PP matrix can be classified as (BC700 > BC600 > BC500 > BC400 > BC300). This later phenomenon of enhanced interface interactions can be correlated to the large surface area, porous structure, and surface chemistry of BC prepared at higher temperatures (Elnour et al., 2019). It is worth highlighting here that in this study no compatibilizer was used for improving the filler-polymer interfacial bonding, which confirms that this trend of enhanced interface quality is merely due to the inherent characteristics of BC type. Moreover; in our previous study we also illustrated the dependence of PP diffusion into BC pores on the type of BC and we showed that the molten PP is infiltrated into the BC pores, which resulted in better mechanical interlocking between the BC particles with the PP matrix, due to the enhanced filler-matrix interface (Tjong, 2012).

3.2. Differential scanning calorimetry (DSC)

The crystalline structure as well as the degree of crystallinity of semi-crystalline polymers can affect the physical and mechanical properties of selected polymer significantly. As mentioned earlier, the crystallinity and crystallization kinetics of semi-crystalline polymers depend mainly on the processing conditions employed and the presence of carbonaceous fillers. During solidification from the melt, carbonaceous fillers can act as heterogeneous nucleation sites for the polymer crystallites. This reduces nucleation activation energy, leading to an acceleration of the crystallization and a decrease of the spherulite size (Elnour et al., 2019).

The thermal behaviors of the neat PP and the BC/PP composite systems are presented in Figs. 2 and 3 for the melting and crystallization peaks respectively. The numerical values of the DSC thermograms were extracted and the results are summarized in Table 1. The heat of melting (ΔH_m) and crystallization heats (ΔH_c) were determined from the areas of melting and crystallization peaks of the DSC thermograms, respectively.

From Fig. 2, it could be noticed that the neat PP showed a typical endothermic melting peak at ~ 163 °C. When BC is incorporated into PP, the melting temperature (T_m) of BC/PP composites is increased compared to the neat PP. This increase in the T_m could be attributed to the heterogeneous nucleation effects exerted by the rigid fillers. Similarly, the crystallization temperatures (T_c) shown in Fig. 3 were also found to relatively increase toward higher temperatures (earlier onset crystallization temperature) for all the composites compared to the neat PP matrix. The BC particles act as points from where crystal growth is initiated. This type of early onset of crystallization temperature, as a result of carbonaceous filler addition, has been noticed and reported in the literature (Wang et al., 2018; Yu et al., 2018; Lin et al., 2018). It is also interesting to observe that crystallization temperature (T_c) increases proportionally with the amount of BC loading in all the composites. This might be related to the increased number of the nucleus that is available during the crystallization process as a result of the increased number of BC particles at higher loadings. Thus, the higher loading of BC particles aids in earlier crystallization of the PP matrix. Similarly, one can observe that at specific loading, BC prepared at higher temperatures induce more crystallization effect into PP, or in other words, the crystallization induction could be classified as (BC700 > BC600 > BC500 > BC400 > BC300). This behavior might be attributed to the higher surface areas and pore volumes of BC prepared at higher temperatures (Table S2). Higher surface area and pore volumes lead to more infiltration of the PP chain into the pores of BC particles and more BC-PP interlocking. A similar observation is also reported in the literature (Bhattacharyya et al., 2003). Another possible reason might be attributed to the BC hydrophobicity (Elnour et al., 2019), which increases with pyrolysis temperature and makes the BC particles more compatible with the hydrophobic PP matrix. Though the difference in the hydrophobicity of the BC prepared at different temperatures is not prominent, however, these factors (surface area,

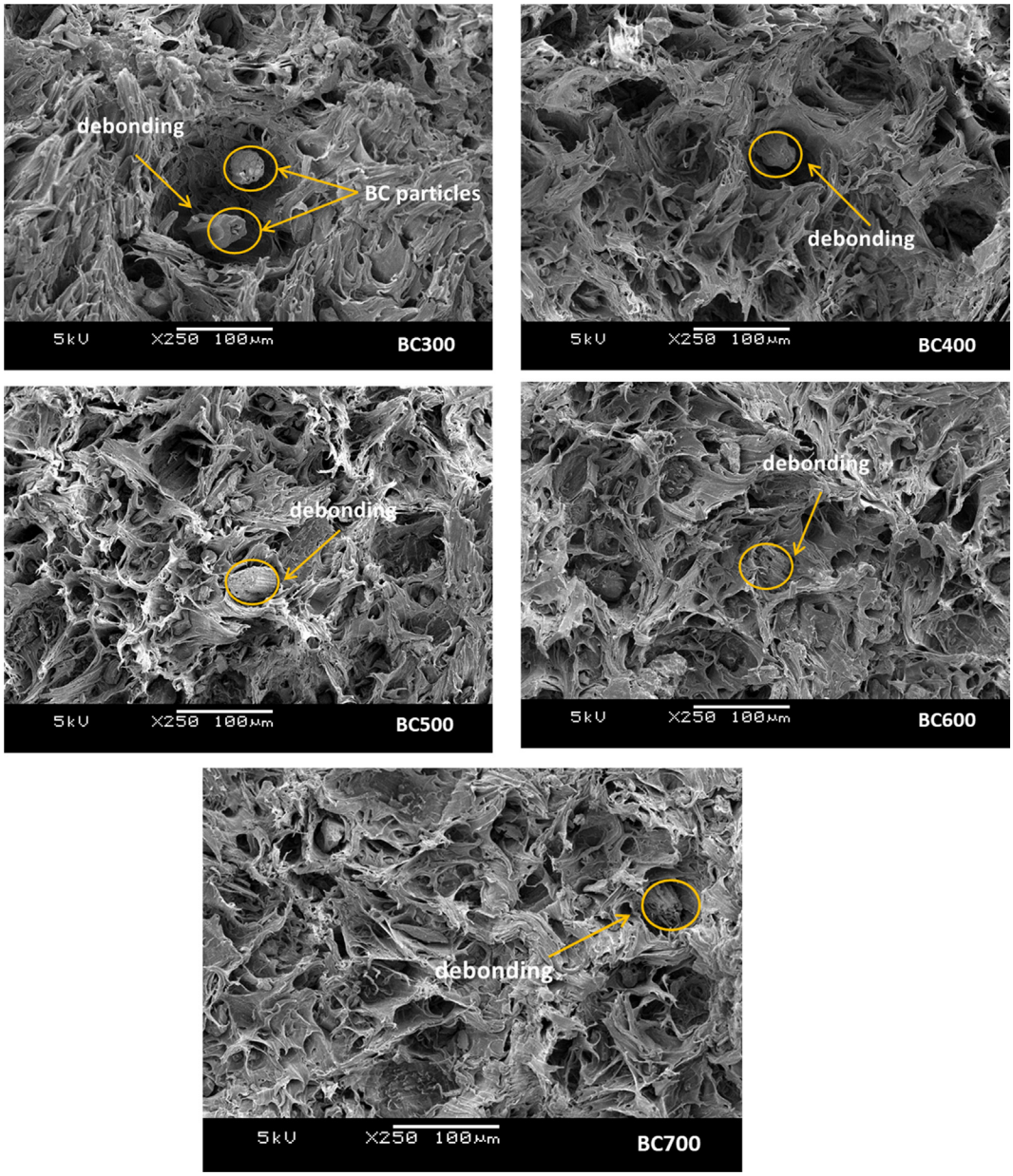

Fig. 1. SEM morphologies of fractured-surface composites at the maximum BC loading (i.e. 20 wt%).

pore-volume, and hydrophobicity) could act synergistically for enhancement of the overall composite crystallization process.

The analysis of the melt crystallization process for different BC types by using Avrami's equation can be very useful for understanding the crystallization kinetics.

It is well acknowledged that the Avrami model is ideally adapted for the prediction and quantification of crystal growth and nucleation under isothermal conditions, numerous studies have also been performed under non-isothermal conditions (Coburn et al., 2018; Kim Piew et al., 1999; Wang and Dou, 2007). This non-isothermal crystallization of semicrystalline polymers closely resembles the industrial melt polymer process.

Fig. 4 presents the relative crystallinity as a function of time for BC/PP composites at fixed BC loading. The BCs are prepared at different temperatures as discussed above. The gradual increase in relative crystallinity as a function of time for these composites can be seen in Fig. 4. Also, sigmoidal curves for all the composites were observed. The added BC type has shown a significant influence on the crystallization kinetics of the PP. From the data, it is deduced that BC addition enhanced the crystallization rate of resulted composites. This is obvious from the fact that the time required to reach a relative crystallinity of 100% became shorter. This effect is more pronounced in the case of composites fabricated with BC prepared at higher temperatures i.e. 500 °C onward. This indicates that the incorporation of BC particles into the PP matrix results in a decreased crystallization time of the PP chains. In other words, the induction time that is required for the overall crystallization process of BC/PP composites has decreased. Moreover, the increased BC concentration has also resulted in a reduced induction time, which suggests the hetero-nucleating action of BC particles. A similar type of effect is reported in the literature with the loading of carbon fillers (Lin et al., 2018; Bhattacharyya et al., 2003; Tian et al., 2017).

Fig. 5 shows the typical Avrami plots of ln $[-\ln(1-\theta(t))]$ versus ln (t)corresponding to the neat PP and BC/PP composites. It can be observed that both neat PP and BC/PP composites are following

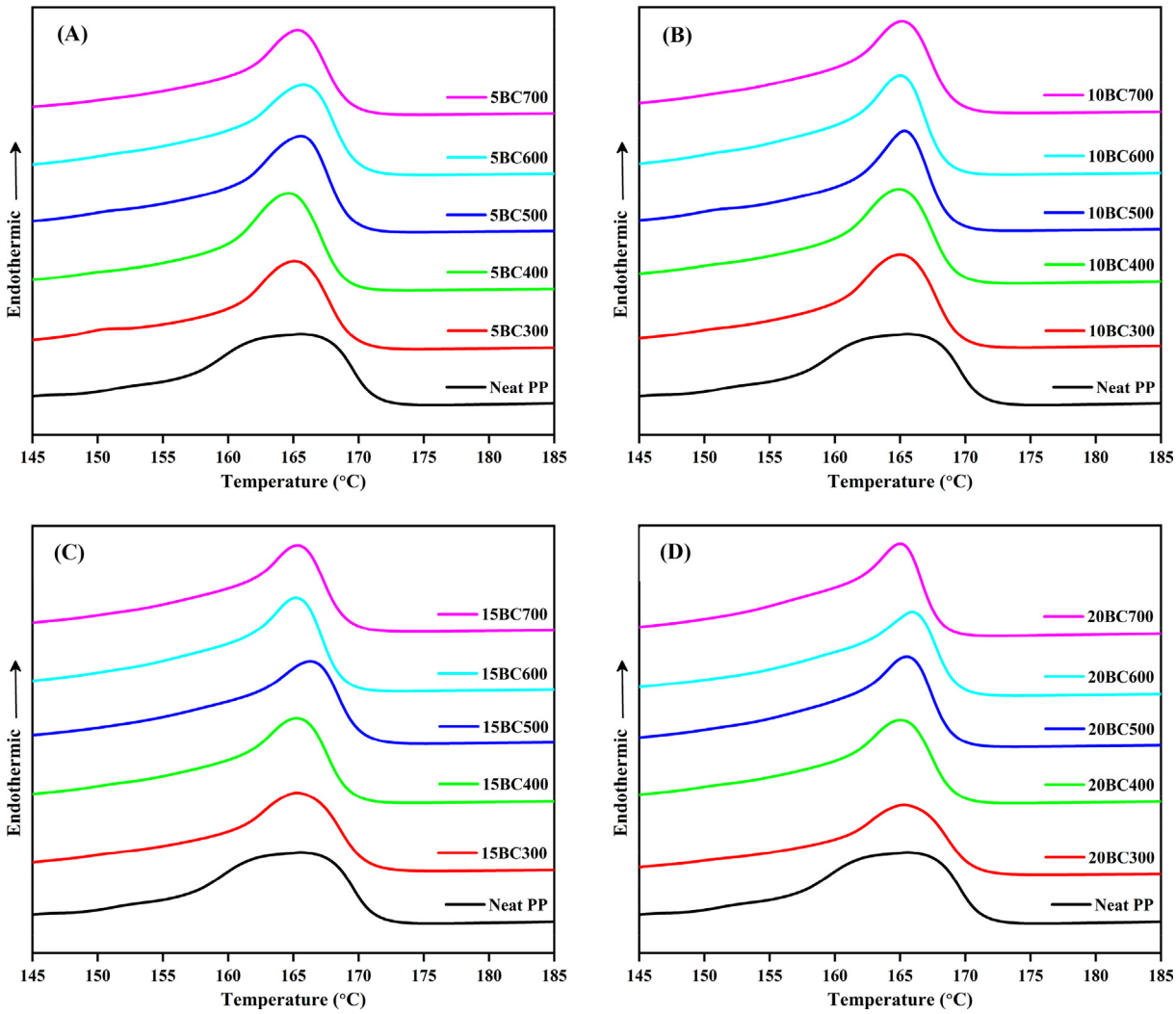

Fig. 2. Melting peaks of BC/PP composites, (A) 5%, (B) 10%, (C) 15% and (D) 20% loading.

Avrami's theory; since very good linearity between ln $[-\ln(1-\theta(t))]$ versus ln (t) was obtained with an excellent correlation coefficient of ($R \geq 0.990$) (Table 2). The yielded Avrami exponent n and crystallization rate constant k are given in Table 2. The value of n for the neat PP and it's BC/PP composites was found to be between 2 and 3, indicating a two-dimensional crystal growth with a linear growth rate (Parija and Bhattacharyya, 2017). Surprisingly, the values of n for BC/PP composites prepared with BC300 and BC400 were higher than that of neat PP. However, the composites prepared with BC500, BC600, and BC700 showed lower n values. This variation in crystallization characteristics might be ascribed to the inherent difference between BC properties prepared at different temperatures. As n value is an indication of the nuclei growth dimensions, the values of $1 \leq n \leq 2$ indicates 1-dimensional rod-like growth, whereas the values of $2 \leq n \leq 3$ indicate 2-dimensional disc-like growth. Therefore, the relatively high porous structure and surface areas of the BC prepared at high-temperature (such as BC500, BC600, and BC700) points towards a 2-dimensional disc-like growth pattern rather than the rod-like pattern. This behavior could be correlated to the fact that PP chains can well penetrate the BC particle prepared at higher temperatures (BC500, BC600, and BC700) and diffuse through pores in BC/PP composites (Elnour et al., 2019).

The Avrami rate constant (k) could be a useful parameter to understand the nucleation and fastening effect of BC particles. The higher k value implies a higher extent of nucleation effect (Parija and Bhattacharyya, 2017). In all the composites, the Avrami rate constant (k) increases as compared to the neat PP, where neat PP showed a k value of 2.93×10^{-5}, while the BC/PP composites exhibited a k value in the range between 2.00×10^{-5} to 2.00×10^{-4}. Besides, it can be observed that the BC prepared at higher temperatures (i.e. BC500, BC600, and BC700) showed the highest k values compared to lower temperature BC when considering the effect of the BC type and its loading percentage. This also justified faster crystallization of the BC/PP composites in comparison with the neat PP. Similarly, another useful parameter for understanding the nucleation and fastening effect of BC particles is the half crystallization time ($t_{1/2}$). This also showed a lower value for BC particles prepared at high temperature compared to the lower one.

In general, the addition of the BC particles into the PP matrix leads to an enhanced crystallization process due to their heterogeneous nucleating effect. This nucleating effect was found to be similar to other carbonaceous fillers reinforced PP composites such as carbon black (Li et al., 2006), single-walled carbon nanotubes

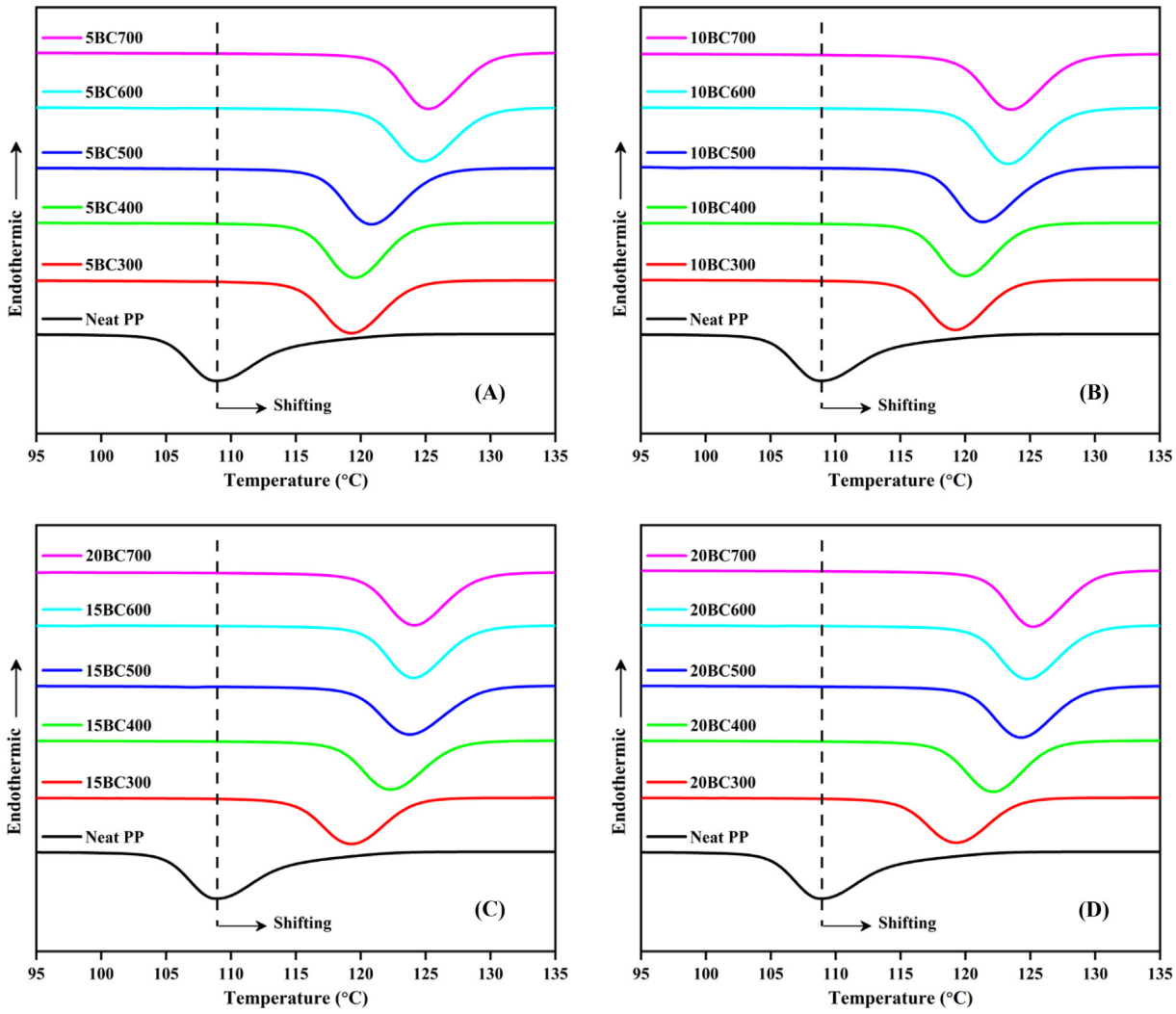

Fig. 3. Crystallization peaks of BC/PP composites, (A) 5%, (B) 10%, (C) 15% and (D) 20% loading.

Table 1
Summarized results of DSC analysis of PP and its BC/PP composites.

Sample		DSC parameters				
		T_c (°C)	ΔH_c (J/g)	T_m (°C)	ΔH_m (J/g)	X_r (%)
Neat PP	109.24	−91.25	163.05	76.2	36.46	
BC300	5BC/PP	119.26	−83.79	165.55	69.27	34.89
	10BC/PP	119.25	−87.90	164.09	71.63	38.10
	15BC/PP	119.35	−84.35	164.43	68.69	38.67
	20BC/PP	119.83	−76.64	163.60	62.75	37.53
BC400	5BC/PP	119.49	−92.47	165.73	74.95	37.75
	10BC/PP	119.98	−90.33	165.32	74.41	39.56
	15BC/PP	122.33	−74.79	166.33	67.69	38.10
	20BC/PP	122.21	−76.26	164.58	64.13	38.36
BC500	5BC/PP	120.78	−83.78	166.17	69.33	34.92
	10BC/PP	121.33	−76.50	165.21	64.42	34.25
	15BC/PP	123.82	−83.50	165.24	71.22	40.10
	20BC/PP	124.21	−83.76	165.35	71.47	42.75
BC600	5BC/PP	121.20	−93.16	165.66	76.48	38.52
	10BC/PP	123.24	−111.01	165.30	92.07	48.95
	15BC/PP	124.13	−90.53	165.38	74.98	42.21
	20BC/PP	124.80	−82.03	165.52	69.9	41.81
BC700	5BC/PP	121.23	−91.14	164.91	76.72	38.64
	10BC/PP	123.53	−75.86	166.03	63.16	33.58
	15BC/PP	124.11	−83.41	165.36	70.71	39.80
	20BC/PP	125.26	−80.97	165.60	68.23	40.81

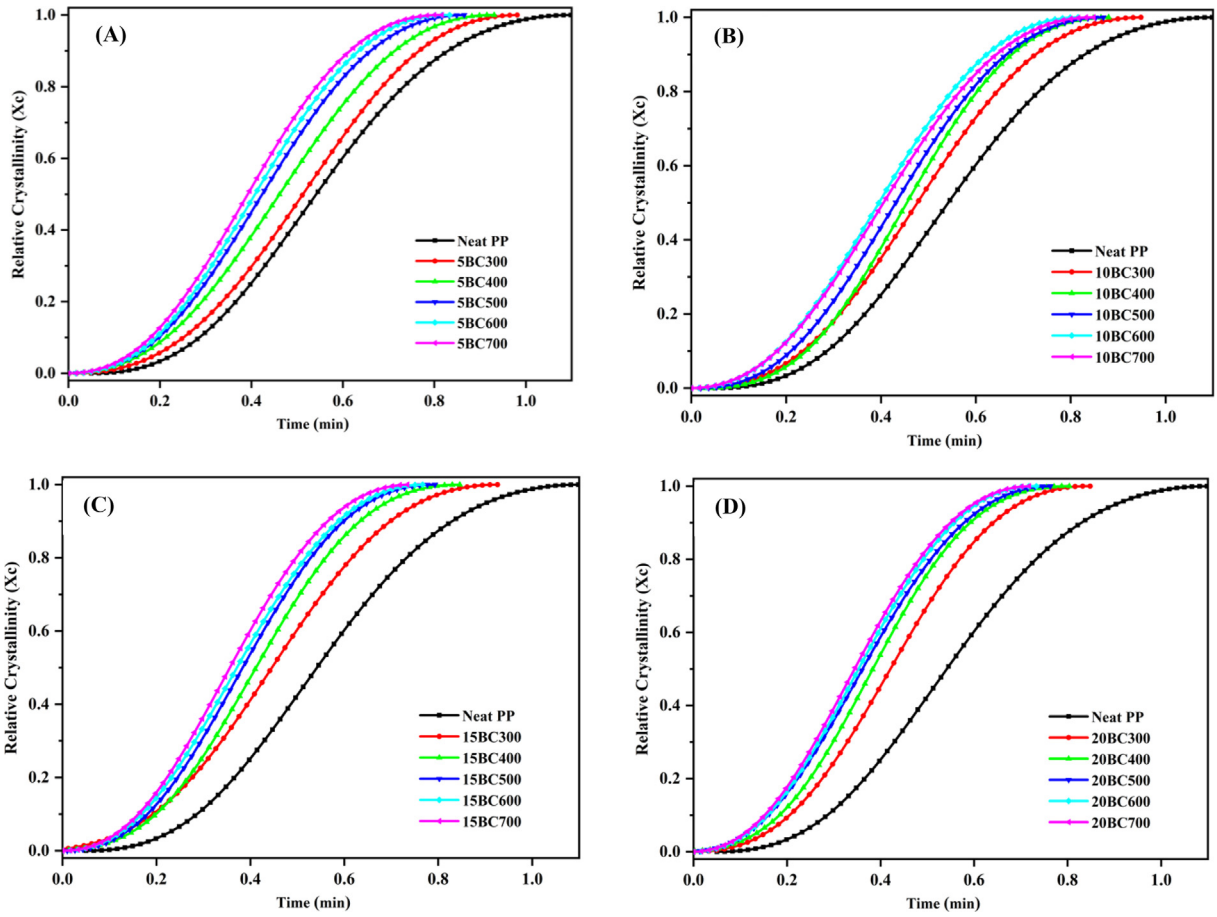

Fig. 4. Relative crystallinity with time of neat PP and BC/PP composites, (A) 5%, (B) 10%, (C) 15%, and (D) 20% loading.

(SWNTs) (Bhattacharyya et al., 2003), Multi-walled Carbon Nanotubes (MWCNTs) (Parija and Bhattacharyya, 2017), and carbon fibers (Tian et al., 2017).

3.3. Spherulite morphology

The analysis of spherulitic growth under optical microscopy was carried out at 120 °C. The selection of this temperature was merely based on the assumption that at a lower temperature, the spherulite growth occurs very rapidly. The morphological evolution of the neat PP sample is shown in Fig. 6I A-D, while that of composite made with 15% loading of BC500 is shown in Fig. 6II (A-D), for comparison. Here we have randomly selected the 15BC500/PP sample just for the sake of brevity, as we believe that in other composites the morphology will be just a duplication. From Fig. 6I(A-D), it can be seen, for neat PP, that the morphological evolution during crystallization at 120 °C, started with very small nuclei that are barely seen, shown as very tiny black dots in Fig. 6(IA), which required about 1 min to emerge. As the crystallization time progresses, at 2 min, it can be observed that the spherulites start to form (Fig. 6I(B)), at time 5 min or less, the neat PP spherulites grow continuously and become fully developed and well recognized at 10 min, which is an indication that the crystallization process is finished.

For the BC/PP composite under study (i.e: 15BC500), It can be seen that at time < 1 min, Fig. 6II (A), nuclei formation is detected, similar to neat PP sample. However, as the crystallization event proceeds further; at a time 2 min or higher (Fig. 6II(B–D) spherulites were observed. These were not similar to the one observed in the case of neat PP sample, rather a vast number of small-sized spherulites were formed. In other words, the number of spherulites developed for the model 15BC500 was significantly higher than the neat PP. This crystallization behavior of the composite could be attributed to the fact that heterogeneous nucleation caused by BC particles prevented homogeneous nucleation of PP, which resulted in the small-sized PP crystallites with fractural (imperfect) morphologies of PP spherulites. Similar behavior was observed for PP composites prepared with MWCNTs (Lin et al., 2018). Overall, this analysis of spherulitic morphology is in well accordance with the conclusions made from the DSC crystallization analysis that the nucleation rate of the BC/PP composites is evidently enhanced when BC is added to the PP matrix, and also the BC particles served as a nucleating agent for the PP matrix, which led to a faster crystallization rate of PP.

3.4. Thermogravimetric analysis (TGA)

Thermal stability of polymeric materials is an important parameter since thermal stability can be a limiting factor in polymer processing as well as its end-use applications (El Achaby et al., 2012). Thermal degradation of PP and BC/PP with different BC weight fractions as well as different BC types (prepared at different temperatures) was determined from the weight loss during heating. The weight loss (TGA) curves are presented in Fig. 7, and derivatives weight loss ((DTG)) are presented in supplementary information (Fig. S2), respectively. From these Figures, the temperature for 5 and 15% weight loss ($T_{5\%}$ and $T1_{5\%}$) and the maximum decomposition temperature (T_{max}) were extracted and the results were

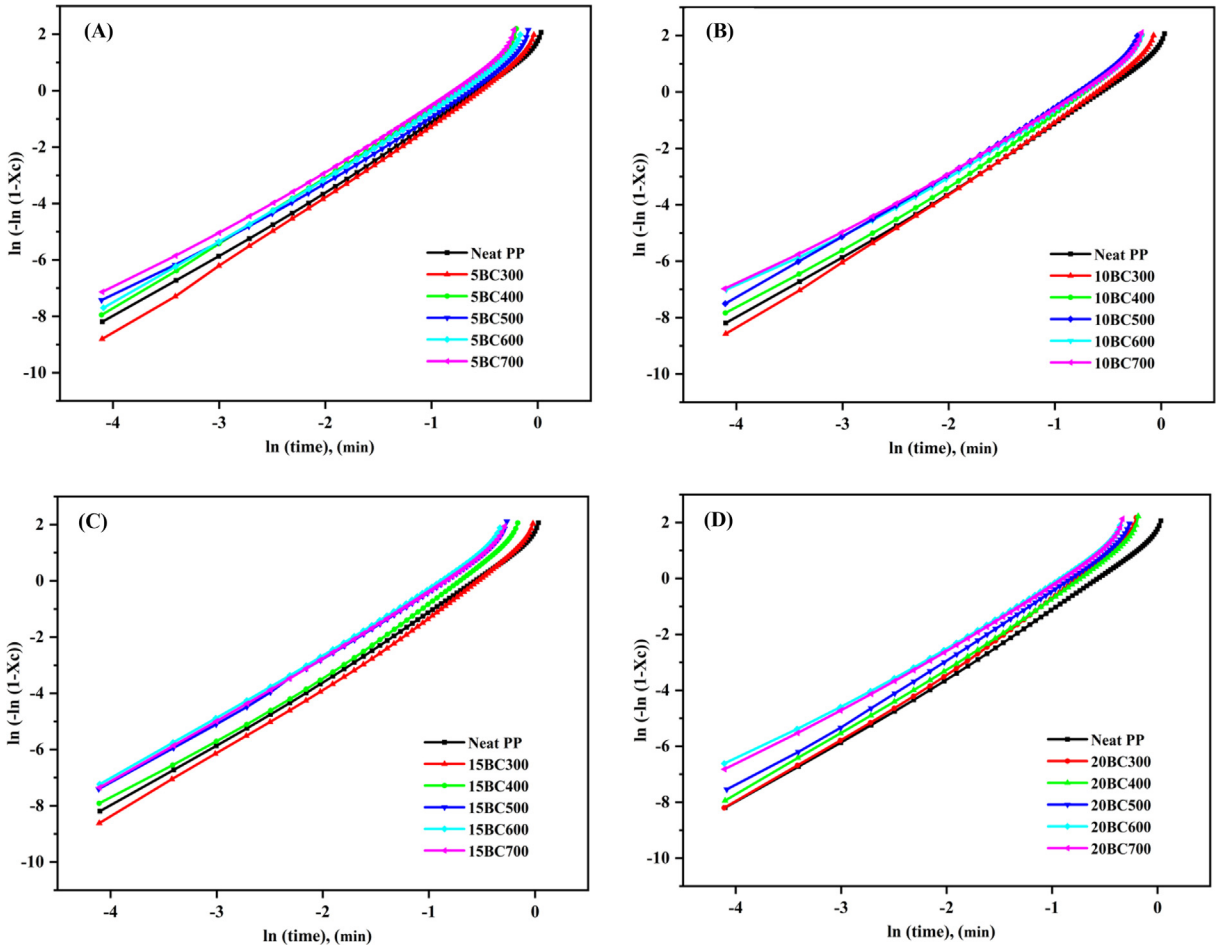

Fig. 5. Avrami plot of neat PP and BC/PP composites, (A) 5%, (B) 10%, (C) 15% and (D) 20% loading.

Table 2
Avrami crystallization parameters of neat PP and its BC/PP composites.

Sample		Avrami parameters			
		n	$k^{(1/n)}$	$t_{(½)}$ (s)	R^2
Neat PP	2.89	2.93E-5	32.60	0.996	
BC300	5BC/PP	2.94	2.95 E-5	30.66	0.995
	10BC/PP	2.96	3.40E-5	28.56	0.992
	15BC/PP	3.07	2.87E-5	26.76	0.991
	20BC/PP	3.11	2.99E-5	25.32	0.992
BC400	5BC/PP	3.05	2.76E-5	27.72	0.995
	10BC/PP	3.02	3.19E-5	27.3	0.997
	15BC/PP	2.95	5.39E-5	24.72	0.992
	20BC/PP	2.78	7.87E-5	22.92	0.992
BC500	5BC/PP	2.97	4.61E-5	25.50	0.989
	10BC/PP	2.84	6.79E-5	25.80	0.990
	15BC/PP	2.80	1.06E-4	23.04	0.988
	20BC/PP	2.75	1.46E-4	21.72	0.997
BC600	5BC/PP	2.78	9.68E-5	24.36	0.994
	10BC/PP	2.78	9.75E-5	24.30	0.994
	15BC/PP	2.68	1.69E-4	22.32	0.995
	20BC/PP	2.68	1.94E-4	21.18	0.992
BC700	5BC/PP	2.78	1.07E-4	23.46	0.991
	10BC/PP	2.80	1.00E-4	23.52	0.990
	15BC/PP	2.73	1.52E-4	21.90	0.995
	20BC/PP	2.71	1.91E-5	20.58	0.990

summarized in Table 3. From Fig. 7, it could be noticed that the thermal degradation of the neat PP and its BC/PP composites occur as a single step process. The maximum decomposition temperature (T_{max}) for the neat PP was recorded at around 467 °C while the weight loss values of 5% ($T_{5\%}$) and 15% ($T_{15\%}$) were recorded at 384 and 422 °C, respectively. Also; it could be seen that all the BC/PP composites have shown a delayed degradation onset temperature compared to the neat PP matrix. This is an indication of

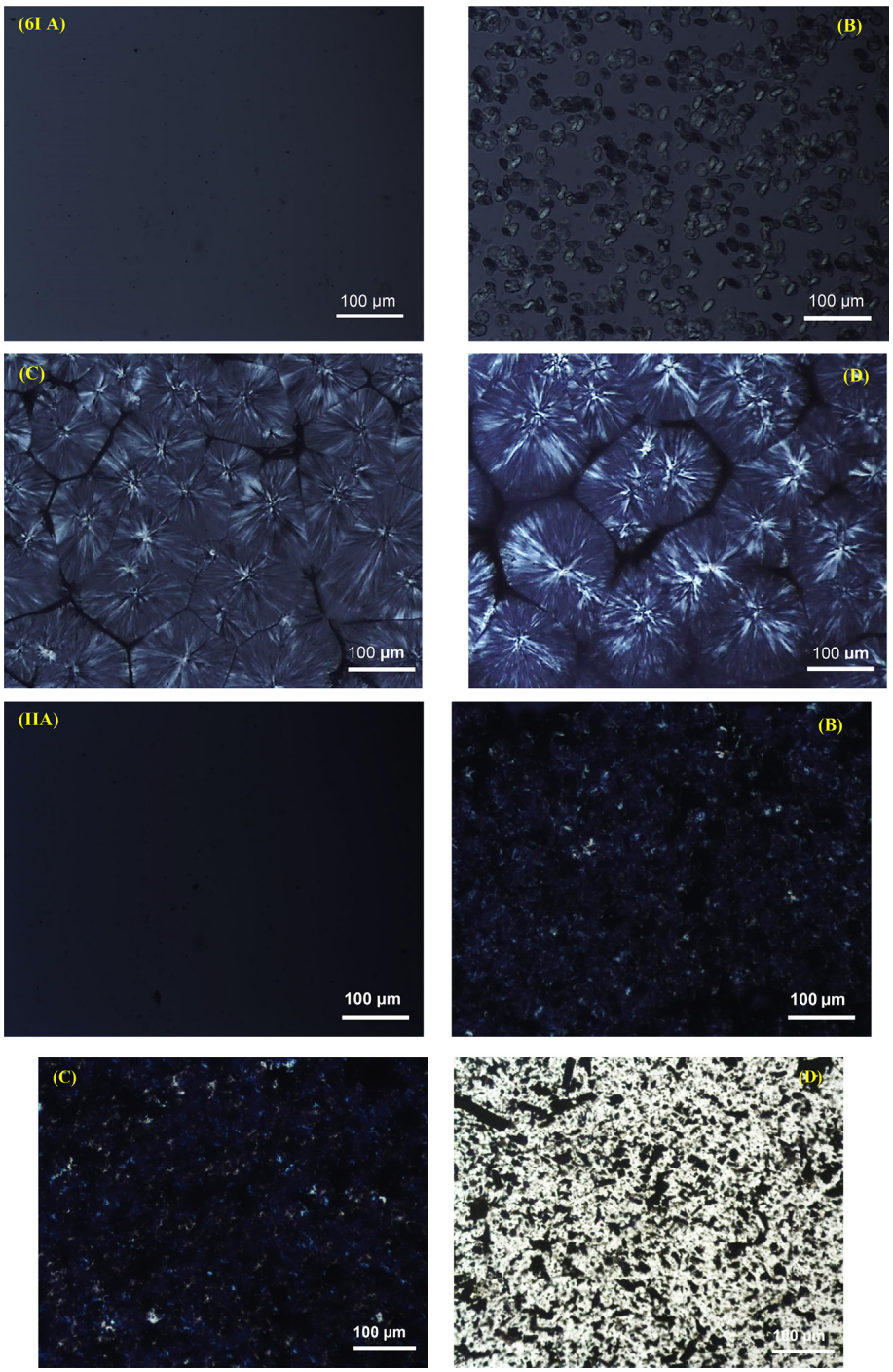

Fig. 6. **(I)** POM images of neat PP at 120 °C, taken at times (A) < 1 min, (B) < 2 min, (C) 5 min and (D) > 10 min and (**II**) POM images of 15BC500/PP composites at 120 °C, images taken at (A) 0 min, (B) 2 min, (C) 5 min and (D) 5 min without cross polarizer.

the improved thermal stability of the composites due to the addition of the thermally stable BC particles. This improvement in the resistance to thermal degradation of the composite can be attributed to the hindered diffusion of volatile decomposition products within the composites due to the barrier effect of the added BC particles (Elnour et al., 2019). Moreover, this causes mass transfer limitations of produced volatile gases, and it is strongly dependent on the BC-PP interactions. The enhancement of thermal stability can also be attributed to the free radical trapping mechanism (Su et al., 2011). The (C–C) bond in the main chains of PP breaks at a high temperature to form carbon-based radicals, also; in the presence of oxygen O_2, the (C–H) bond can be attacked by O_2 to generate (HO•) and alkoxy free radicals (RO•) and subsequently leads to a series of polymer chain degradations through random scission. However; the addition of BC can delay the degradation of PP chains by trapping these generated free radicals from further propagation. Fig. S3(A) in supplementary information shows the residual weight percentage of BC/PP composites, it could be observed that the BC residue produced after each degradation cycle was proportional to the amount of BC added to the PP matrix. This effect was more pronounced in the composites having a higher amount of BC particles in them. Additionally, Fig. S3(B) presents the maximum degra-

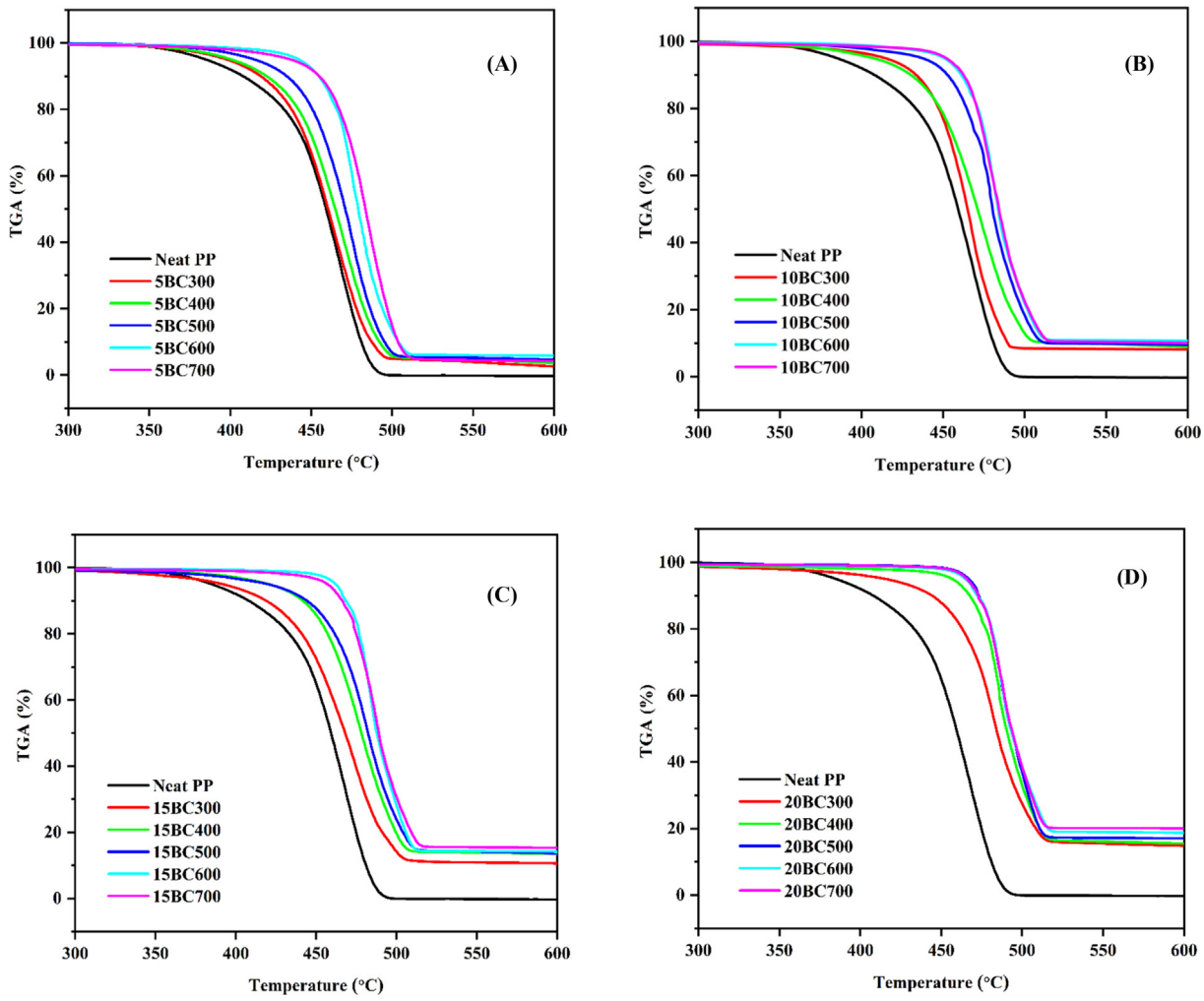

Fig. 7. TGA curves of BC/PP composites, (A) 5%, (B) 10%, (C) 15% and (D) 20% loading.

Table 3
Summarized results of TGA analysis ($T_{5\%}$, $T_{15\%}$, and T_{max}) of PP and its BC/PP composites.

Sample		TGA			DTG
		$T_{5wt\%}$ [a] (°C)	$T_{15wt\%}$ [b] (°C)	Residual %	T_{max} [c] (°C)
Neat PP	384.56	422.57	0	467.31	
BC300	5BC/PP	391.72	430.04	2.57	467.43
	10BC/PP	398.05	441.86	8.10	467.84
	15BC/PP	414.59	431.92	10.62	471.92
	20BC/PP	415.56	455.85	14.80	485.23
BC400	5BC/PP	400.80	434.54	3.58	470.80
	10BC/PP	407.32	440.84	8.86	474.80
	15BC/PP	420.26	450.76	13.48	480.37
	20BC/PP	456.72	473.06	15.47	488.98
BC500	5BC/PP	415.01	444.52	4.55	475.01
	10BC/PP	437.29	454.75	9.51	480.28
	15BC/PP	419.77	459.63	13.64	483.97
	20BC/PP	466.94	477.80	17.02	490.44
BC600	5BC/PP	442.28	461.11	5.81	480.97
	10BC/PP	450.47	466.43	10.71	483.31
	15BC/PP	461.58	472.09	14.15	485.82
	20BC/PP	464.56	478.45	18.69	490.45
BC700	5BC/PP	437.51	462.34	4.17	486.36
	10BC/PP	451.84	467.79	10.05	487.18
	15BC/PP	456.87	474.09	15.80	488.38
	20BC/PP	465.97	477.91	20.03	490.82

[a] $T_{5wt\%}$ represents the temperature at which 5 wt% weight loss rate occurred, [b]$T_{15wt\%}$ represents the temperature at which 15 wt% weight loss rate occurred and [c]T_{max} represented the temperature at which the maximum weight loss rate occurred.

dation temperature (T_{max}) of BC/PP composites as a function of BC particles loading. It is clear from the figure that T_{max} increases gradually for all composite with loading, however, the trend of increase varies for the BC type. Furthermore, when comparing different types of BC at a particular loading, it is can be deduced that the thermal stability of BC/PP composites following the order of BC700 > BC600 > BC500 > BC400 > BC300. Thus, from the TGA experiments, it can be concluded that the addition of BC particles to PP enhances the thermal stability of PP by delaying the composites onset decomposition and its maximum temperatures along with producing a high amount of BC residues. Such important characteristics might widen the application spectrum of BC/PP composites; whenever thermal stability is a key factor. For instance, the application of composites where fire retardation property is a key consideration. Moreover, the as-prepared BC/PP composites exhibit good thermal stability in the range where polymer processing is performed. Thus BC can be incorporated into a PP matrix by melt blending without any noticeable degradation.

4. Conclusion

BC-reinforced PP composites were successfully prepared by melt processing technique and the effect of BC type (based on pyrolysis temperature) on the composite's crystallization kinetics, crystalline structure, and thermal stability was investigated. DSC results revealed that BC particles act as a nucleating agent for crystallization. Furthermore, the incorporation of BC particles into the PP matrix enhanced the overall crystallization process, indicated by the shifting of crystallization temperatures (T_c) toward higher values (early crystallization onset). The results obtained from the studies of crystallization kinetics showed that the overall rates of crystallization, as well as the rate of nucleation, were higher for BC/PP composites as compared to near PP matrix. It is reaching ten times higher, indicating that BC particles served as a nucleating agent for the PP matrix. POM analysis of spherulite morphology was in well accordance with the conclusion made from the DSC crystallization analysis. That the nucleation rate of the BC/PP composites is evidently enhanced when BC is added to the PP. TGA results indicated that the addition of BC particles into the PP matrix enhances the thermal stability up to 80℃ for specific BC/PP composite by delaying both the onset decomposition as well as maximum degradation temperatures.

CRediT authorship contribution

Abdulaziz A. Algayamah: Methodology, Funding acquisition. **Ahmed Yagoub Elnour:** Investigation, Data curation. **Hamid Shaikh:** Conceptualization, Visualization, Original Draft Preparation, Writing - review & editing. **Sajjad Haider:** Formal analysis. **Anesh Manjaly Poulose:** Validation. **S.M. Al-Zahrani:** Resources. **Waheed A. Almasry:** Supervision. **Soo Young Park:** Resources.

Declaration of Competing Interest

The authors declare that they have no known competing financial interests or personal relationships that could have appeared to influence the work reported in this paper.

Acknowledgements

The authors extend their appreciation to the Deanship of Scientific Research at King Saud University for funding this work through research group no (RG-1440-060). The authors would also like to thanks to SABIC Polymer Research Center (SPRC) for providing the necessary facilities.

Appendix A. Supplementary data

Supplementary data to this article can be found online at https://doi.org/10.1016/j.jksus.2021.101409.

References

Pudełko, A., Postawa, P., Stachowiak, T., Malińska, K., Dróżdż, D., 2021. Waste derived biochar as an alternative filler in biocomposites-mechanical, thermal and morphological properties of biochar added biocomposites. J. Cleaner Prod. 278, 123850. https://doi.org/10.1016/j.jclepro.2020.123850.

Adeniyi, A.G., Abdulkareem, S.A., Ighalo, J.O., Onifade, D.V., Adeoye, S.A., Sampson, A. E., 2020. Morphological and thermal properties of polystyrene composite reinforced with biochar from elephant grass (Pennisetum purpureum). J. Thermoplast. Compos. Mater. https://doi.org/10.1177/0892705720939169.

Zhang, Q., Zhang, D., Xu, H., Lu, W., Ren, X., Cai, H., Lei, H., Huo, E., Zhao, Y., Qian, M., 2020. Biochar filled high-density polyethylene composites with excellent properties: towards maximizing the utilization of agricultural wastes. Ind. Crops Prod. 146, 112185. https://doi.org/10.1016/j.indcrop.2020.112185.

Elnour, A.Y., Alghyamah, A.A., Shaikh, H.M., Poulose, A.M., Al-Zahrani, S.M., Anis, A., Al-Wabel, M.I., 2019. Effect of pyrolysis temperature on biochar microstructural evolution, physicochemical characteristics, and its influence on biochar/polypropylene composites. Appl. Sci. 9 (6), 1149. https://doi.org/10.3390/app9061149.

Giorcelli, M., Khan, A., Pugno, N.M., Rosso, C., Tagliaferro, A., 2019. Biochar as a cheap and environmental friendly filler able to improve polymer mechanical properties. Biomass Bioenergy 120, 219–223. https://doi.org/10.1016/j.biombioe.2018.11.036.

Poulose, A.M., Elnour, A.Y., Anis, A., Shaikh, H., Al-Zahrani, S.M., George, J., Al-Wabel, M.I., Usman, A.R., Ok, Y.S., Tsang, D.C.W., Sarmah, A.K., 2018. Date palm biochar-polymer composites: An investigation of electrical, mechanical, thermal and rheological characteristics. Sci. Total Environ. 619–620, 311–318. https://doi.org/10.1016/j.scitotenv.2017.11.076.

Behazin, E., Misra, M., Mohanty, A.K., 2017. Sustainable biocarbon from pyrolyzed perennial grasses and their effects on impact modified polypropylene biocomposites. Compos. B Eng. 118, 116–124. https://doi.org/10.1016/j.compositesb.2017.03.003.

Das, O., Sarmah, A.K., Bhattacharyya, D., 2016. Biocomposites from waste derived biochars: mechanical, thermal, chemical, and morphological properties. Waste Manage. 49, 560–570. https://doi.org/10.1016/j.wasman.2015.12.007.

Das, O., Bhattacharyya, D., Sarmah, A.K., 2016. Sustainable eco–composites obtained from waste derived biochar: a consideration in performance properties, production costs, and environmental impact. J. Cleaner Prod. 129, 159–168. https://doi.org/10.1016/j.jclepro.2016.04.088.

Ikram, S., Das, O., Bhattacharyya, D., 2016. A parametric study of mechanical and flammability properties of biochar reinforced polypropylene composites. Compos. Part A: Appl. Sci. Manuf. 91, 177–188. https://doi.org/10.1016/j.compositesa.2016.10.010.

Mileva, D., Tranchida, D., Gahleitner, M., 2018. Designing polymer crystallinity: an industrial perspective. Polym. Crystal. 1 (2), e10009. https://doi.org/10.1002/pcr2.10009.

Turgut, G., Işıksel, E., Kahraman, G., Eren, T., Özkoç, G., 2018. Synthesis of phosphorus-and phenyl-based ROMP polymers and investigation of their effects on the thermomechanical and flammability properties of a polypropylene–IFR system. J. Appl. Polym. Sci. 135 (11), 45998. https://doi.org/10.1002/app.45998.

Wang, C.C., Zhao, Y.Y., Ge, H.Y., Qian, R.S., 2018. Enhanced mechanical and thermal properties of short carbon fiber reinforced polypropylene composites by graphene oxide. Polym. Compos. 39 (2), 405–413. https://doi.org/10.1002/pc.23950.

Yu, Y., Zeng, F., Chen, J., Kang, J., Yang, F., Cao, Y., Xiang, M., 2018. Isothermal crystallization kinetics and subsequent melting behavior of β-nucleated isotactic polypropylene/graphene oxide composites with different ordered structure. Polym. Int. 67 (9), 1212–1220. https://doi.org/10.1002/pi.5625.

Zheng, Y., Chen, Y., 2017. Preparation of polypropylene/Mg–Al layered double hydroxides nanocomposites through wet pan-milling: formation of a second-staging structure in LDHs intercalates. RSC Adv. 7 (3), 1520–1530. https://doi.org/10.1039/C6RA26050K.

Cai, L., Dou, Q., 2019. Investigation on the melting and crystallization behaviors, mechanical properties and morphologies of polypropylene/sericite composites. J. Mater. Sci. 54 (4), 3600–3618. https://doi.org/10.1007/s10853-018-3049-y.

Lin, Z.-I., Lou, C.-W., Pan, Y.-J., Hsieh, C.-T., Huang, C.-L., Chen, C.-K., Lin, J.-H., 2018. PP/MWCNTs composites: effects of length of MWCNTs on isothermal crystallization behaviors, crystalline structure, and thermal stability. J. Compos. Mater. 52 (4), 503–517. https://doi.org/10.1177/0021998317710084.

Beuguel, Q., Boyer, S.A., Settipani, D., Monge, G., Haudin, J.M., Vergnes, B., Peuvrel-Disdier, E., 2018. Crystallization behavior of polypropylene/graphene nanoplatelets composites. Polym. Crystal. 1 (3), e10024. https://doi.org/10.1002/pcr2.10024.

ASTM D3418-15, 2015. Standard Test Method for Transition Temperatures and Enthalpies of Fusion and Crystallization of Polymers by Differential Scanning Calorimetry, ASTM International, West Conshohocken, PA. www.astm.org.

Wunderlich, B., 1990. Thermal Analysis. Academic Press, pp. 417–431.
Li, Y., Wang, S., Zhang, Y., Zhang, Y., 2006. Crystallization behavior of carbon black-filled polypropylene and polypropylene/epoxy composites. J. Appl. Polym. Sci. 102 (1), 104–118. https://doi.org/10.1002/app.23254.
ASTM E1131-20, 2020. Standard Test Method for Compositional Analysis by Thermogravimetry, ASTM International, West Conshohocken, PA. www.astm.org.
Tjong, S.C., 2012. Polymer Composites with Carbonaceous Nanofillers: Properties and Applications. John Wiley & Sons.
Bhattacharyya, A.R., Sreekumar, T., Liu, T., Kumar, S., Ericson, L.M., Hauge, R.H., Smalley, R.E., 2003. Crystallization and orientation studies in polypropylene/single wall carbon nanotube composite. Polymer 44 (8), 2373–2377. https://doi.org/10.1016/S0032-3861(03)00073-9.
Coburn, N., Douglas, P., Kaya, D., Gupta, J., McNally, T., 2018. Isothermal and non-isothermal crystallization kinetics of composites of poly(propylene) and MWCNTs. Adv. Industr. Eng. Polym. Res. 1 (1), 99–110. https://doi.org/10.1016/j.aiepr.2018.06.001.
Kim Piew, C., Gan, S.N., Chee, K.K., 1999. Determination of avrami exponent by differential scanning calorimetry for non-isothermal crystallization of polymers. Polymer 40 (1), 253–259. https://doi.org/10.1016/S0032-3861(98)00188-8.
Wang, J., Dou, Q., 2007. Non-isothermal crystallization kinetics and morphology of isotactic polypropylene (iPP) nucleated with rosin-based nucleating agents. J. Macromol. Sci. Part B 46 (5), 987–1001. https://doi.org/10.1080/00222340701457311.
Tian, H., Zhang, S., Ge, X., Xiang, A., 2017. Crystallization behaviors and mechanical properties of carbon fiber-reinforced polypropylene composites. J. Therm. Anal. Calorimetr. 128 (3), 1495–1504. https://doi.org/10.1007/s10973-016-5996-3.
Parija, S., Bhattacharyya, A.R., 2017. Multiwalled carbon nanotubes-based polypropylene composites: Influence of interfacial interaction on the crystallization behavior of polypropylene. Polym. Eng. Sci. 57 (2), 183–196. https://doi.org/10.1002/pen.24399.
El Achaby, M., Arrakhiz, F.E., Vaudreuil, S., el Kacem Qaiss, A., Bousmina, M., Fassi-Fehri, O., 2012. Mechanical, thermal, and rheological properties of graphene-based polypropylene nanocomposites prepared by melt mixing. Polym. Compos. 33 (5), 733–744. https://doi.org/10.1002/pc.22198.
Su, S., Xu, Y., Wilkie, C., 2011. Thermal degradation of polymer–carbon nanotube composites. In: Polymer–Carbon Nanotube Composites. Elsevier, pp. 482–510.